JAAS

ROYAL SOCIETY OF CHEMISTRY

PAPER

Cite this: *J. Anal. At. Spectrom.*, 2020, **35**, 510

In situ sequential U–Pb age and Sm–Nd systematics measurements of natural LREE-enriched minerals using single laser ablation multi-collector inductively coupled plasma mass spectrometry†

Chao Huang,[ab] Yue-Heng Yang,*[abc] Lie-Wen Xie,[abc] Shi-Tou Wu,[ab] Hao Wang,[ab] Jin-Hui Yang[abc] and Fu-Yuan Wu[abc]

Received 15th October 2019
Accepted 9th December 2019

DOI: 10.1039/c9ja00346k

rsc.li/jaas

In the present work, we describe a sequential U–Pb and Sm–Nd systematics measurement from natural LREE-enriched minerals using Neptune Plus MC-ICP-MS coupled with a 193 nm excimer laser in a single shot. MC-ICP-MS is equipped with an optical zoom lens to bring ion beams into the collector coincidently. The key features allow rapid switching between the U–Pb and Sm–Nd collector configurations, which are applied to simultaneously measure the U–Pb age and Sm–Nd isotope of common natural LREE-enriched minerals. The robustness and usefulness of the present protocol are investigated using a series of well-characterized mineral reference materials (*i.e.*, monazite, titanite, perovskite) with known U–Pb and Sm–Nd isotopic values, which demonstrate its potential and versatility in geochemistry and cosmochemistry for microanalysis.

1. Introduction

U–Pb and Sm–Nd systematics have widespread applications in geochemistry and cosmochemistry, both in geochronology and in provenance/tracer studies. In the last decade, a notable increase in the precision and accuracy of the U–Pb and Sm–Nd systems has been achieved for some LREE-enriched accessory minerals by LA-ICP-MS, especially the successful use of MC-ICP-MS with LA. Compared to the single collector quadrupole or magnetic sector-field ICP-MS (Q-ICP-MS or SF-ICP-MS), the feature of a simultaneous static detection system offered by MC-ICP-MS provides high quality analytical data as well as accuracy and precision far superior to the one achieved by Q-ICP-MS or SF-ICP-MS. The advantages comprise (1) high-efficiency detection and spatial resolution and (2) high resistance to spectral skew and flicker noise from the plasma source or ablated particles, which lead to the acquisition of lower internal and external uncertainties in isotopic ratios.[1–4] Owing to its superiority, LA-MC-ICP-MS is now widely accepted as the most sensitive and versatile analytical tool for isotopic analysis in geochronology and isotopic geochemistry (*e.g.*, U–Pb, Lu–Hf and/or Sm–Nd isotopic measurements) at high spatial resolution even though it shows less preponderance than SIMS when measuring the U–Pb age.[5–9]

Despite the above-described advantages, there are still challenges posed by the U–Pb dating and Sm–Nd isotopic ratios of accessory LREE-enriched minerals when studying complex zonation minerals, small crystal domains and detrital/inherited minerals by LA-MC-ICP-MS. In this case, geochemical information (*e.g.*, age, isotope ratio and trace element) is stored in tiny crystal domains, and these various types of information from a single ablation crater should be undoubtedly desirable for research workers. Previously, the most commonly used approach for obtaining spatially resolved information from the isotopic distributions of geological samples was to carry out two separate analytical processes: first retrieving the U–Pb age, followed by the measurement of the Lu–Hf or Sm–Nd isotopic ratios. In this case, the information provided by two separate analyses is not obtained from the same volume of the material, which can result in the de-coupling of the age-isotope system and inaccurate initial isotopic compositions.[10,11]

To resolve the above-described limitations, an analytical technique (*in situ* simultaneous analysis using laser ablation split stream; LASS) was presented by Xie *et al.*,[12] combining a laser with more than one MS system. The first simultaneous measurements of trace elements including U–Pb data by Q-ICP-MS and Lu–Hf isotope by MC-ICP-MS for zircon were reported

[a]*State Key Laboratory of Lithospheric Evolution, Institute of Geology and Geophysics, Chinese Academy of Sciences, Beijing 100029, P. R. China. E-mail: yangyueheng@mail.iggcas.ac.cn*

[b]*Innovation Academy of Earth Science, Chinese Academy of Sciences, Beijing 100029, P. R. China*

[c]*College of Earth and Planetary Sciences, University of Chinese Academy of Sciences, Beijing 100049, P. R. China*

† Electronic supplementary information (ESI) available. See DOI: 10.1039/c9ja00346k

by Yuan *et al.*[13] The LASS technique allows the simultaneous isotopic ratio measurements of the same single ablation volume, preserving the original information and the spatial relationship between key chronological and geochemical tracer records.[10–23] In addition to the LASS technique, a quasi-simultaneous approach was proposed as an alternative technique. In 2004, with the use of this method, the measurement of the zircon $^{207}Pb/^{206}Pb$ age and Hf isotope composition was first launched by Woodhead *et al.*,[24] followed by Harrison *et al.*[25] and Kemp *et al.*[26] Unfortunately, the determination of the U–Pb age was unsuccessful for its inapplicability to Phanerozoic zircons. Subsequently, Xia *et al.*[27] improved the method by exploiting a Nu Plasma HR MC-ICP-MS, allowing the concordance of the measured ages to be assessed, Pb loss to be identified, and physical mixing of the cores and rims during analysis to be noted.[4] More recently, Craig *et al.* proposed a rapid response laser ablation technology for the U–Pb age and Hf isotope ratio analysis using the quasi-simultaneous approach afforded by a Thermo Scientific Neptune XT MC-ICP-MS coupled with an Elemental Scientific Lasers NWR 193 laser ablation system.[28]

Considering the limitation of the simultaneous zircon U–Pb and Lu–Hf systematics by MC-ICP-MS, the aim of this work is to present a quasi-simultaneous U–Pb and Sm–Nd systematics measurement in common natural LREE-enriched minerals using a MC-ICP-MS connected to a 193 nm excimer laser in a single shot. The proposed methodology is validated and investigated to measure well-characterized mineral reference materials (*i.e.*, monazite, titanite and perovskite) with known U–Pb age and Sm–Nd isotopic ratios, indicating its potential and versatility in geochemistry and cosmochemistry for microanalysis.

2. Experimental

2.1 Instrumentation

Experiments of all accessory minerals investigated in this study were conducted on a Neptune Plus MC-ICP-MS (Thermo Fisher Scientific, Germany) coupled with a 193 nm ArF excimer laser ablation system (GeolasHD, Coherent, USA) at the State Key Laboratory of Lithospheric Evolution, the Institute of Geology and Geophysics, Chinese Academy of Sciences (IGG, CAS), Beijing. A detailed description of the instrumentation can be found in previous studies.[29,30]

In this study, the laser fluence was set to 5–9 J cm^{-2} with laser repetition rate set to 6–10 Hz, and the spot sizes ranged from 16 μm to 90 μm, all depending on the U, Pb and Nd concentrations in the samples. Helium was used as the carrier gas within the ablation cell. Nitrogen gas was added to the carrier gas at 4 mL min^{-1} through a three-way tube to enhance the sensitivity.[31,32] The detailed instrumental operating conditions are presented in Table 1.

Furthermore, the magnet of the Neptune Plus was laminated for high speed and low hysteresis and allowed fast peak jumping, and the shortest time needed for the magnetic field and the Faraday cup to settle could be 0.1 s when jumping from one mass to another. Depending on these characteristics, the method proposed in this study could be established for the simultaneous detection of the U–Pb and Sm–Nd isotopes.

Table 1 Typical instrumental operating conditions, data acquisition parameters and depth of laser pits

Mass spectrometry (Neptune Plus MC-ICP-MS)	
RF forward power	1200 W
Cool gas	16 L min^{-1}
Auxiliary gas	0.8 L min^{-1}
Sample gas	Ar: ~1.0 L min; N_2: 4 mL min^{-1}
Cones	Nickel standard sample cone; X skimmer cone (Ni)
Integration times	(1) U–Pb: 0.066 s, 400 cycles, including the first 100 s for blank in one block; (2) Sm–Nd: 0.131 s, 200 cycles in one block
Acquired isotopes	(1) ^{206}Pb (L4), ^{207}Pb (L3),$^{220.57}M$ (C), ^{238}U (H4); (2) ^{143}Nd (L2), ^{144}Nd (L1), ^{146}Nd (C), ^{147}Sm (H1), ^{149}Sm (H2)
Laser ablation system (Geolas HD)	
Laser	COMPex Pro 102, ArF Excimer, 193 nm
Energy	5 J cm^{-2} for monazite and perovskite; 9 J cm^{-2} for titanite
Spot size	(1) 16 μm for Jefferson; (2) 32 μm for Diamantina; (3) 16 μm for RW-1; (4) 24 μm for Namaqualand; (5) 90 μm for Ontario and OLT; (6) 60 μm for AFK and 10AFK-2
Carrier gas	0.72 L min^{-1} (He)
Repetition rate	6 Hz for monazite and perovskite; 10 Hz for titanite
Depth	(1) 10AFK-2 (perovskite): 27.540 μm; (2) OLT-1 (titanite): 57.848 μm; (3) Namaqualand (monazite): 32.830 μm with a spot size of 24 μm; (4) Namaqualand (monazite): 30.406 μm with a spot size of 90 μm

2.2 Analytical protocol

Details of the instrumental setup and measurement conditions are summarized in Tables 1 and 2. Two analytical modes, the static and dynamic measurements, are offered by the Neptune Plus.[30] A static measurement is a method that uses only a single line within the cup configuration table. All required isotopic currents are collected simultaneously, and the magnetic field is not changed during the analysis. However, only nine isotopes can be measured simultaneously when using the static mode. In the case of dynamic measurements, the magnetic field is switched for every line and different isotopic currents are focused into the detectors.

In this study, the dynamic model is used for executing the analysis of quasi-simultaneous detection of isotopes by a MC-ICP-MS connected to a LA in a single shot. As shown in Table 2, the two-cup configuration lines were set up. Line 1 was used for the U–Pb age measurement, and the Sm–Nd isotopic ratio measurement was conducted using the other line. One run of measurements consists of one block with one circle. This is because the process of magnetic field switching for every line in each circle is time-consuming when multiple circles are taken. First, the U–Pb age was measured using the line 1 configuration, where 400 integration numbers were used to guarantee the analysis accuracy, and the integration time was set to 0.066 s. Therefore, each U–Pb spot analysis consisted of an approximate

Table 2 Faraday cup configuration of Neptune plus for U–Pb age and Sm–Nd isotope ratio measurement

Line	Cup	L4	L3	L2	L1	C	H1	H2	H3	H4
1	U–Pb	^{206}Pb	^{207}Pb			220.57				^{238}U
2	Sm–Nd			^{143}Nd	^{144}Nd	^{146}Nd	^{147}Sm	^{149}Sm		

9 s background and 17 s sample data acquisition. Subsequently, the Sm–Nd isotopic ratio measurements were conducted using the line 2 configuration, where a total of 200 integration numbers were applied for the sample data collection, and 0.131 s was selected for the integration time. A magnet switching settle time was set to 3 s between the two-cup configuration lines in one run to ensure the stability of the magnetic field. Based on the described details, the time required for each spot was approximately 55 s.

Prior to analysis, the Neptune Plus MC-ICP-MS parameters were optimized using a solution containing 200 ppb of U and Pb for the U–Pb age, and a JNdi-1 standard solution for the Sm–Nd isotopic ratios to achieve an optimal peak shape and maximum sensitivity. Following that, the instrument was connected to a LA, and tuned using NIST SRM 610 glass. Helium was used as the carrier gas mixed with argon gas and sensitivity enhancement gas (nitrogen) before entering the ICP torch. The parameters of these gases were also tuned for optimal sensitivity and fractionation by monitoring the signal intensities of ^{238}U, ^{207}Pb, ^{206}Pb and ^{146}Nd. The detailed parameter settings of MC-ICP-MS and LA are presented in Table 1.[29,30,33–36]

2.3 Data reduction

For the off-line data processing of the U–Pb age measurements, we used the software program ICPMSDataCal9.0.[37] A detailed description of the calculations for the standard deviation of the average isotopic ratio for each analysis, in addition to the correction method for the time-dependent drifts of the U–Pb isotopic ratios using a linear interpolation, is described in Liu *et al.*,[37] The weighted mean U–Pb ages and Concordia plots were processed using the Isoplot3.0 software package.[38] As for *in situ* Sm–Nd isotopic measurements, the data reduction has been previously described in detail by Yang *et al.* and Ma *et al.*;[9,33,39] therefore, herein, only a brief description of the data reduction procedure is provided. The isobaric interference of ^{144}Sm on ^{144}Nd is significant. We used the measured ^{147}Sm/^{149}Sm ratio to calculate the Sm fractionation factor. The interference-corrected ^{146}Nd/^{144}Nd ratio can then be used to calculate the Nd fractionation factor. Finally, the ^{147}Sm/^{144}Nd and ^{143}Nd/^{144}Nd ratios were normalized using the exponential law.[9,33,34,37,39]

3. Results and discussion

In order to validate the present protocol, we present an *in situ* sequential U–Pb age and Sm–Nd isotope analysis for well-characterized mineral reference materials (*e.g.*, monazite, titanite and perovskite) with known U–Pb age and Sm–Nd isotope compositions. For detailed information of the analytical data, see the ESI Tables 1 and 2.†

3.1 Monazite reference materials: Jefferson, Diamantina, Namaqualand and RW-1

Four monazite samples previously well characterized by Liu *et al.* (2012)[43] were analyzed. In this study, 44 069 monazite was used as the primary reference material, which came from an upper amphibolite-facies psammitic paragneiss from the Wilmington Complex, Delaware, USA. The sample yielded a TIMS Concordia age of 424.9 ± 0.4 Ma.[40]

The Jefferson monazite came from the Bigger Mica Mine, Jefferson County, Colorado, USA, which yielded a mean ID-TIMS ^{206}Pb/^{238}U age of 364 Ma.[41] Using the LA-MC-ICP-MS method, Peterman *et al.*[41] reported a ^{206}Pb/^{238}U age of 365.5 ± 2.6 Ma (2σ), and Alagna *et al.*[42] obtained a Concordia age of 362.1 ± 3.8 Ma (2σ, n = 12) with a weighted mean ^{206}Pb/^{238}U age of 362.3 ± 4.4 Ma (2σ, n = 12), and Liu *et al.*[43] achieved a weighted mean ^{206}Pb/^{238}U age of 365.2 ± 2.6 Ma (2σ, n = 32). However, the result of the CA-TIMS analysis revealed the complex age patterns of the Jefferson monazite with a maximum ^{206}Pb/^{238}U age of 382.1 ± 0.4 Ma, and a minimum ^{206}Pb/^{238}U age of 363.9 ± 0.5 Ma.[44] The Jefferson U–Pb dating results obtained in this study are showed in Fig. 1a. The 24 analyses were all close to concordant and yielded a weighted mean ^{206}Pb/^{238}U age of 381.1 ± 2.3 Ma (2σ, n = 24, MSWD = 0.2), which is well within the error of the CA-TIMS age reported by Peterman.[44] The ^{147}Sm/^{144}Nd ratios of the Jefferson monazite ranged from 0.5055 to 0.5105. The ^{143}Nd/^{144}Nd isotope results for this monazite varied from 0.513017 to 0.513107 with a mean value of 0.513064 ± 48 (2SD, n = 24; Fig. 1b), consistent with the published value of 0.513057 ± 93 (2SD, n = 39).[43]

The Diamantina Monazite came from Espinhaço Range, SE Brazil with low-U and Low-Th. The weighted mean ^{206}Pb/^{238}U age of 495.26 ± 0.54 Ma (95% confidence, n = 8) was acquired by ID-TIMS.[45] The LA-Q-ICP-MS analysis yielded a weighted mean ^{206}Pb/^{238}U age of 494 ± 2 Ma (95% confidence, MSWD = 0.31, n = 36).[45] The LA-SF-ICP-MS analysis yielded a weighted mean ^{206}Pb/^{238}U age of 492 ± 2 Ma (95% confidence, MSWD = 1.3, n = 21). The U–Pb age acquired by LA-MC-ICP-MS gave a weighted mean ^{206}Pb/^{238}U age of 495 ± 3 Ma (95% confidence, MSWD = 0.94, n = 19).[45] Twenty-six analyses of the Diamantina monazite produced a weighted mean ^{206}Pb/^{238}U age of 494.3 ± 1.0 Ma (2σ, n = 26, MSWD = 0.7) (Fig. 1c). The results are in good agreement with the published ID-TIMS and LA-(MC)-ICP-MS data. Sm–Nd isotope ratios of twenty-six laser spots are shown in Fig. 1d. The ^{147}Sm/^{144}Nd ratios of the Diamantina monazite ranged from 0.1219 to 0.1290. The ^{143}Nd/^{144}Nd

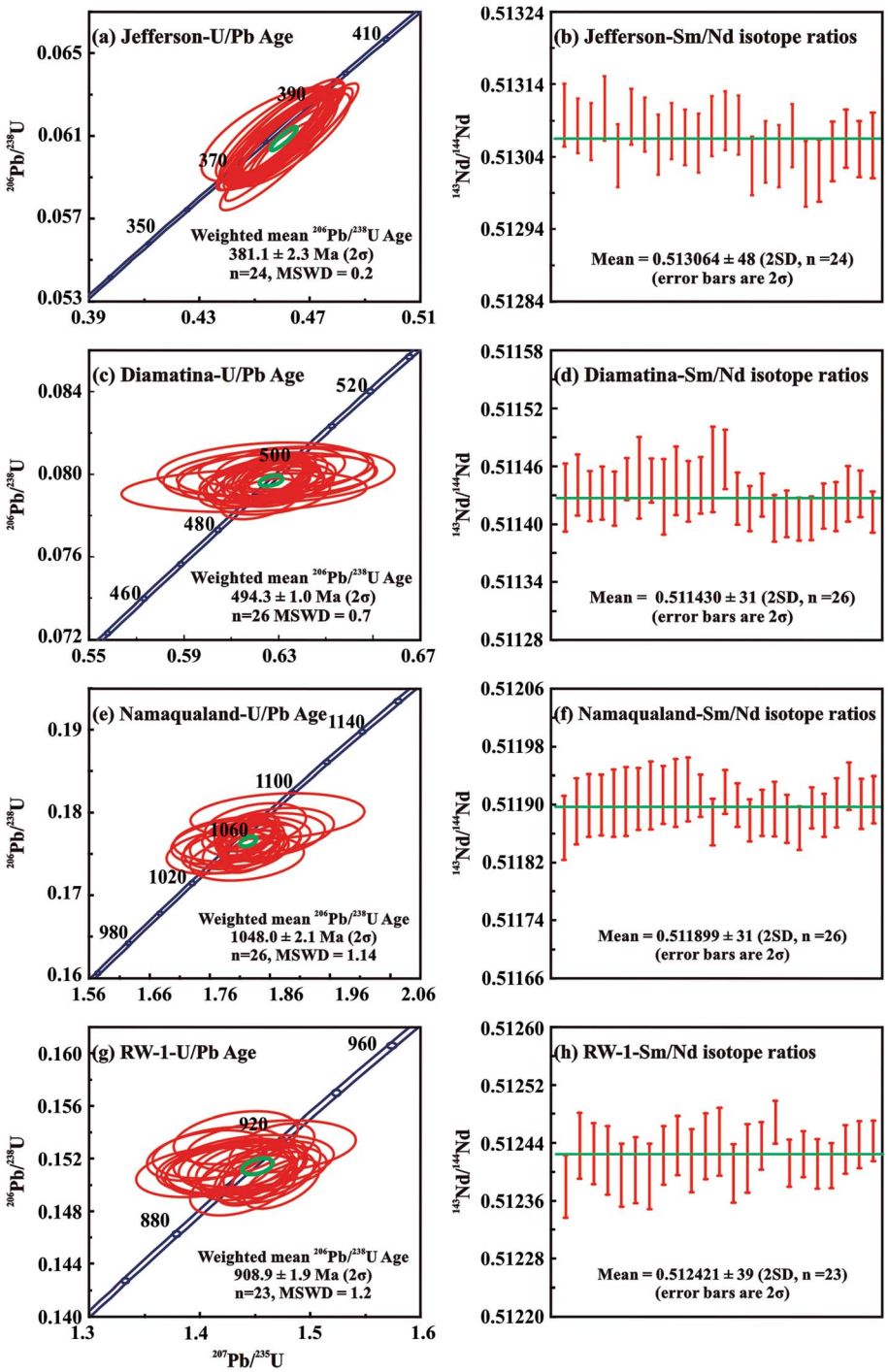

Fig. 1 U–Pb age (Concordia diagrams, error ellipses represent 2σ uncertainties) and $^{143}Nd/^{144}Nd$ isotope ratio of *in situ* sequential analysis for four well-characterized U–Pb and Sm–Nd monazite reference materials. (a and b) Jefferson; (c and d) Diamantina; (e and f) Namaqualand; (g and h) RW-1.

isotope results for this monazite varied from 0.511405 to 0.511467, with a mean of 0.511430 ± 31 (2SD, $n = 26$), which is consistent with the published value of 0.511427 ± 23 (2SD, $n = 60$).[45]

The Namaqualand monazite came from the Steenkampskraal monazite vein in southern Bushmanland, South Africa. A weighted mean $^{207}Pb/^{206}Pb$ age of 1062 ± 14 Ma (2σ, $n = 31$) is achieved by LA-Q-ICP-MS with a younger weighted mean $^{206}Pb/^{238}U$ age of 1046.5 ± 7.1 Ma (2σ, $n = 33$).[43] Two sessions of the Namaqualand monazite measurement were carried out in this study (Fig. 1e). In session 1, eleven analyses gave a weighted mean $^{207}Pb/^{206}Pb$ age of 1060 ± 26 Ma (2σ, $n = 11$) with an MSWD = 0.23, and the corresponding weighted mean $^{206}Pb/^{238}U$ age was 1048.7 ± 5.6 Ma (95% confidence, $n = 11$,

MSWD = 1.9), which is younger. In session 2, fifteen analyses offered a weighted mean $^{207}Pb/^{206}Pb$ age of 1067 ± 11 Ma (2σ, n = 15) with an MSWD = 1.04, and a younger weighted mean age for $^{206}Pb/^{238}U$ of 1047.7 ± 2.6 Ma (2σ, n = 15, MSWD = 0.67) was attained. The two sessions pooled together gave a weighted mean age $^{207}Pb/^{206}Pb$ age of 1066 ± 10 Ma (2σ, n = 26) with an MSWD = 0.68, and a weighted mean $^{206}Pb/^{238}U$ age of 1048.0 ± 2.1 Ma (2s, n = 26, MSWD = 1.14). The results provided by the two sessions were identical to the published value obtained using LA-Q-ICP-MS. The measurement of the Sm–Nd isotope ratios in the two sessions yielded a mean $^{143}Nd/^{144}Nd$ of 0.511903 ± 28 (2SD, n = 11) and 0.511895 ± 32 (2SD, n = 15). A total of twenty-six individual analyses in two sessions yielded a mean $^{143}Nd/^{144}Nd$ of 0.511899 ± 31 (2SD, n = 26; Fig. 1f), which is consistent with the published value of 0.511896 ± 32 (2SD, n = 39) by LA-MC-ICP-MS within analytical error.[43]

The RW-1 monazite came from a pegmatite dyke located in the Landsverk 1 quarry situated in the Evje-Iveland district, South Norway.[46] A previous ID-TIMS analysis on this monazite by Ling *et al.* produced a weighted mean $^{207}Pb/^{235}U$ age of 904.15 ± 0.26 Ma (95% confidence).[46] The dating results by SIMS yielded a weighted mean $^{206}Pb/^{238}U$ age of 906.6 ± 1.5 Ma (2SE, MSWD = 0.74). In this study, twenty-three analyses conducted on the RW-1 monazite yielded a weighted mean $^{207}Pb/^{235}U$ age of 909.4 ± 3.3 Ma (2σ, n = 23, MSWD = 0.90), which was slightly older (at 0.6%) compared to the ID-TIMS age. The acquired weighted mean $^{206}Pb/^{238}U$ age of 908.9 ± 1.9 Ma (2σ, n = 23, MSWD = 1.20; Fig. 1g) is identical to the reference value by SIMS within analytical error.[46] The corresponding Sm–Nd analysis gave a mean $^{147}Sm/^{144}Nd$ of 0.1807 ± 86 (2SD, n = 23) and $^{143}Nd/^{144}Nd$ of 0.512421 ± 39 (2SD, n = 23), as shown in Fig. 1h.

3.2 Titanite reference materials: OLT-1 and Ontario

Two titanite reference materials (OLT-1 and Ontario) were analyzed as unknown samples, and BLR-1 titanite reference materials were used as the primary standard with a CA-TIMS weighted mean $^{206}Pb/^{238}U$ age of 1047.1 ± 0.4 Ma,[39] which is from the Bear Lake Diggings locality, near Tory Hill, Ontario, Canada.[47]

The OLT-1 titanite was sampled at Otter Lake, Quebec, within the Grenville Province of the Canadian Shield. The sample yielded a concordant ID-TIMS age of 1014.8 ± 2.0 Ma (2σ, n = 6, MSWD = 1.8) with a weighted mean $^{206}Pb/^{238}U$ ages of 1014.5 ± 2.4 Ma (95% confidence, n = 6, MSWD = 3.0).[48] Sun *et al.* reported ^{207}Pb-corrected weighted mean $^{206}Pb/^{238}U$ ages of 1015 ± 5 Ma (2σ, n = 24) and 1017 ± 6 Ma (2σ, n = 24) by LA-Q-ICP-MS using single spot and line raster scan modes, respectively.[49] Ma *et al.* gave a ^{207}Pb-corrected weighted mean $^{206}Pb/^{238}U$ age of 1011 ± 6 Ma (2σ, n = 21) by LA-Q-ICP-MS.[39] Twenty analyses of the OLT-1, in this study, yielded a U–Pb Tera–Wasserburg Concordia lower intercept age of 1014.1 ± 4.4 Ma with a MSWD of 0.23 (Fig. 2a), consistent with the ^{207}Pb-corrected weighted mean $^{206}Pb/^{238}U$ age of 1014.9 ± 4.5 Ma (2σ, n = 20, MSWD = 0.04). A $^{207}Pb/^{206}Pb$ value of 0.9099 was used to anchor the lower intercept in light of the Stacey and Kramers terrestrial Pb evolution model. This age is accurate within the uncertainty of the ID-TIMS age.[50] The Sm–Nd

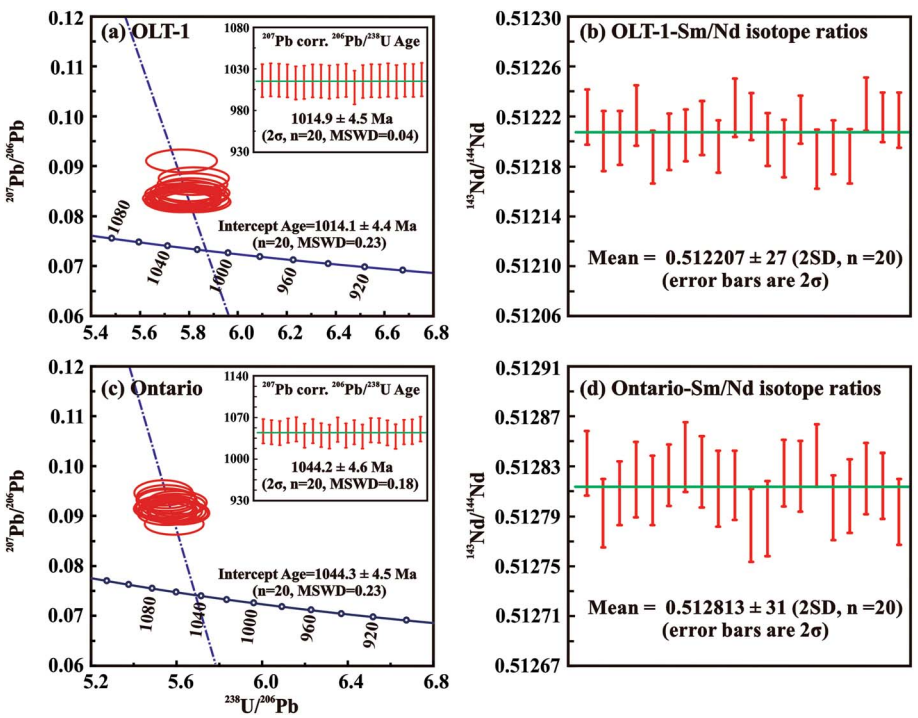

Fig. 2 U–Pb age (Tera–Wasserburg Concordia diagrams anchored through common Pb and ^{207}Pb-corrected weighted mean $^{206}Pb/^{238}U$ age, error ellipses represent 2σ uncertainties) and $^{143}Nd/^{144}Nd$ isotope ratio of *in situ* sequential analysis for two well-characterized U–Pb and Sm–Nd Titanite reference materials. (a and b) OLT-1; (c and d) Ontario.

analysis yielded a mean $^{147}Sm/^{144}Nd$ value of 0.1249 ± 7 (2SD, n = 20) and $^{143}Nd/^{144}Nd$ of 0.512207 ± 27 (2SD, n = 20) as shown in Fig. 2b, which is consistent with the published value of 0.512214 ± 41 (2SD, n = 184) by LA-MC-ICP-MS within analytical error.[39]

The Ontario titanite came from the Renfrew district of Ontario, Canada, which has an ID-TIMS $^{206}Pb/^{238}U$ age of 1053.3 ± 3.1 Ma (95% confidence, n = 6).[51] Sun *et al.* carried out a detailed LA-Q-ICP-MS analysis, yielding a ^{207}Pb-corrected weighted mean $^{206}Pb/^{238}U$ age of 1056 ± 5 Ma (2σ, n = 28, MSWD = 0.3).[49] Ma *et al.* acquired consistent lower intercept and weighted mean $^{206}Pb/^{238}U$ ages of 1047 ± 6 Ma (2σ, n = 21).[39] In this study, twenty analyses of the Ontario titanite yielded a U–Pb Tera–Wasserburg Concordia lower intercept age of 1044.3 ± 4.5 Ma with an MSWD = 0.18 (Fig. 2c), consistent with the ^{207}Pb-corrected weighted mean $^{206}Pb/^{238}U$ age of 1044.2 ± 4.6 Ma (2σ, n = 20, MSWD = 0.18). A $^{207}Pb/^{206}Pb$ value of 0.9131 was used to anchor the lower intercept in light of the Stacey and Kramers terrestrial Pb evolution model.[49] This age is slightly younger, at 0.9%, compared to the ID-TIMS age. The Sm–Nd analysis yielded a mean $^{147}Sm/^{144}Nd$ value of 0.1940 ± 9 (2SD, n = 20) and $^{143}Nd/^{144}Nd$ of 0.512813 ± 31 (2SD, n = 20) as shown in Fig. 3d, which is consistent with the published value of 0.512815 ± 0.000041 (n = 145, 2SD) by LA-MC-ICP-MS within analytical error.[39] In addition, the measured $^{143}Nd/^{144}Nd$ value is consistent with the value of 0.512833 ± 8 (2SD, n = 4) using ID-MC-ICP-MS.[39]

3.3 Perovskite reference materials: AFK and 10AFK-2

Two perovskite samples were analyzed. TAZ3 and AFK perovskites were used as the primary standards for the two samples. The TAZ3 yielded a TIMS age of 463 ± 2 Ma, and the AFK yielded a $^{206}Pb/^{238}U$ weighted average age of 381.6 ± 1.4 Ma.[52]

The AFK perovskite was from an irregular pegmatite body collected from the Afrikanda complex in the Kola Peninsula, Russia.[52] A lower intercept age of 379.6 ± 9.9 Ma (n = 4) was obtained using ID-TIMS, with a ^{207}Pb-corrected weighted mean $^{206}Pb/^{238}U$ age of 378.6 ± 4.1 Ma (n = 4).[52] The analysis of SIMS for AFK gave a lower intercept age of 385 ± 15 Ma (n = 38) with a ^{207}Pb-corrected weighted mean $^{206}Pb/^{238}U$ age of 383.5 ± 3.5 Ma (n = 38).[52] Twenty-three analyses of the AFK, in this study, yielded a U–Pb Tera–Wasserburg Concordia lower intercept age of 380.7 ± 1.7 Ma with an MSWD of 0.23 (Fig. 3a), consistent with the ^{207}Pb-corrected weighted mean $^{206}Pb/^{238}U$ age of 380.6 ± 1.9 Ma (2σ, n = 23, MSWD = 0.17). A $^{207}Pb/^{206}Pb$ value of 0.8611 was used to anchor the lower intercept in light of the Stacey and Kramers terrestrial Pb evolution model. This age is accurate within the uncertainty of the ID-TIMS age. The Sm–Nd analysis yielded a mean $^{147}Sm/^{144}Nd$ value of 0.0782 ± 47 (2SD, n = 23) and $^{143}Nd/^{144}Nd$ of 0.512590 ± 42 (2SD, n = 23), as shown in Fig. 3b, which is consistent with the published value of 0.512609 ± 27 (2SD, n = 6) by TIMS within analytical error.[52]

The 10AFK-2 perovskite was also extracted from an irregular pegmatite body collected from the Afrikanda complex in the Kola Peninsula, Russia.[52] A lower intercept age of 377 ± 11 Ma

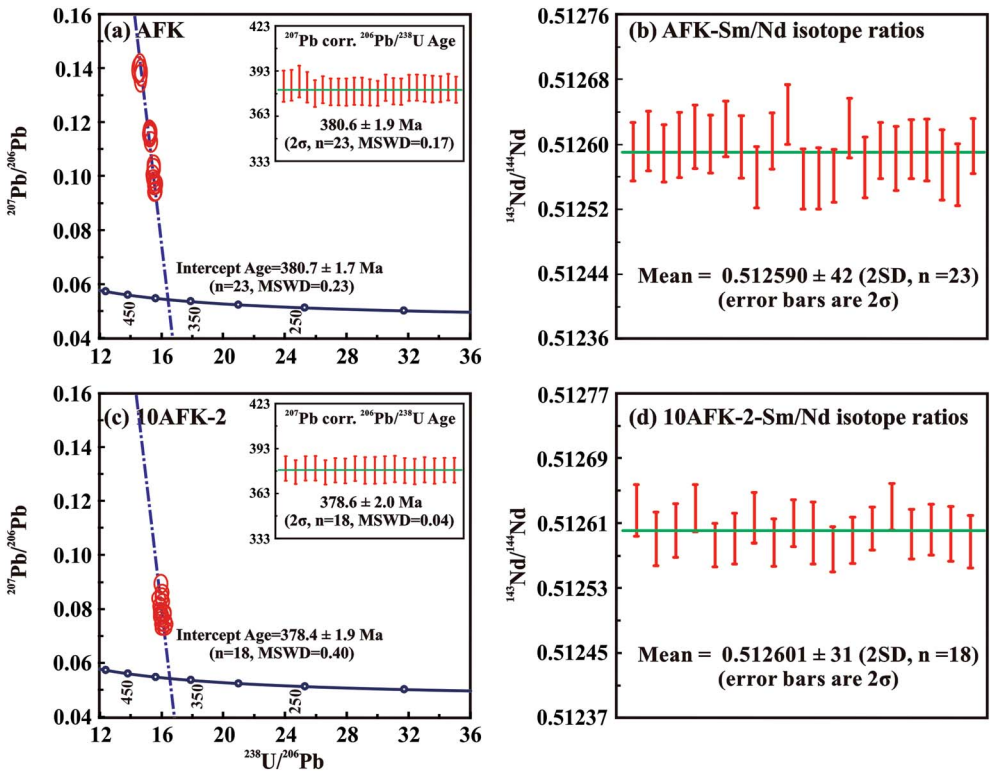

Fig. 3 U–Pb age (Tera–Wasserburg Concordia diagrams anchored through common Pb and ^{207}Pb-corrected weighted mean $^{206}Pb/^{238}U$ age, error ellipses represent 2σ uncertainties) and $^{143}Nd/^{144}Nd$ isotope ratio of *in situ* sequential analysis for two perovskite samples from Kola peninsula, Russia. (a and b) AFK; (c and d) 10AFK-2.

($n = 20$) was obtained using LA-Q-ICP-MS, with a ^{207}Pb-corrected weighted mean ^{206}Pb/^{238}U age of 379.3 ± 4.9 Ma (n = 20).[52] Eighteen analyses of the 10AFK-2 perovskite, in this study, yielded a U–Pb Tera–Wasserburg Concordia lower intercept age of 378.4 ± 1.9 Ma with an MSWD = 0.40 (Fig. 3c), consistent with the ^{207}Pb-corrected weighted mean ^{206}Pb/^{238}U age of 378.6 ± 2.0 Ma (2σ, n = 18, MSWD = 0.04).[52] A ^{207}Pb/^{206}Pb value of 0.8611 was used to anchor the lower intercept in light of the Stacey and Kramers terrestrial Pb evolution model. This age is accurate within the uncertainty of the published age. The Sm–Nd analysis yielded a mean ^{147}Sm/^{144}Nd value of 0.0676 ± 80 (2SD, n = 18) and ^{143}Nd/^{144}Nd of 0.512601 ± 31 (2SD, n = 18) as shown in Fig. 3d, which is consistent with the published value of 0.512612 ± 10 (2SD) by LA-MC-ICP-MS within analytical uncertainties.[52]

3.4 Advantages and limitations

Laser ablation split stream (LASS) has become a routine or popular technique for the measurement of trace elements, U–Pb and Hf or Nd isotopes in zircon and monazite since 2008.[10,12,13,21–23] Nevertheless, considering the requirement of more than one mass spectrometer (MS) exerts a severe restriction to the feasibility of LASS, our *in situ* sequential analysis of the U–Pb age and Sm–Nd isotope from the same volume of material brings an ideal solution to the limitations mentioned above. Comparatively, the present protocol almost maximizes the amount of useful isotopic data that can be obtained from a single spot analysis using one MS instrument. The capability of this analytical protocol when studying complex zonation minerals, small crystal domains and detrital/inherited minerals is presented, especially for natural minerals with enriched Nd contents, such as monazite, titanite, perovskite, allanite, bastnaesite, xenotime and schorlomite. These minerals also are ideal for U–Pb dating.[39,43,46,52]

Nevertheless, considering the Faraday cup for all data acquired in this work, the main limitation of sequential analysis is the signal strength with a slightly larger laser beam size. For this reason, not all minerals are suitable using our protocol due to their lower element concentrations. Only the minerals with high concentrations of Nd and appropriate U and Pb concentrations can be used for the sequential analysis of the U–Pb age and Sm–Nd isotopic ratios with reasonable analytical precision. As stated in a previous study, the deviation requirement for practical geological application is $\pm 2\varepsilon$ units, corresponding to a ^{143}Nd/^{144}Nd data deviation of ±0.0001.[53–55] According to our study, more than about 1500 ppm of Nd is enough for most Nd enriched accessory minerals (*e.g.*, monazite, titanite, perovskite, allanite, bastnaesite, xenotime and schorlomite).[55–58]

In addition, the depth profiling analysis of the laser pit was conducted to demonstrate the advantage of the proposed method over the commonly used approach of two separate analytical processes, which largely depends on the analytical hole depth. The data set of the depth-profiling analysis on three mineral samples demonstrated that, when using the same laser shots (258 pulses, 43 seconds) and energy fluence (5 J cm^{-2}), the depths of the laser pits are almost identical as shown in Table 1. Furthermore, in light of the acquired data set, a thin section thicker than 60 μm could be analyzed by the proposed method. A detailed depth-profiling analysis of the laser pit for each mineral sample is given in the online ESI text.†

4. Conclusions

In this study, we developed a methodology of sequential analysis of the U–Pb age and Sm–Nd isotope in natural LREE-enriched minerals by means of a MC-ICP-MS connected to a 193 nm excimer laser in a single shot. The U–Pb age and Sm–Nd isotope ratios for three common natural LREE-enriched minerals (*e.g.*, monazite, titanite and perovskite) obtained by this method are identical to the reference values within analytical uncertainties, indicating the feasibility and capability of the present method. Our technique is of value in applications requiring the U–Pb age and Sm–Nd isotope ratios from a single laser crater. Thus, the afforded technique provides a powerful tool for petrogenetic studies, indicating the potential and versatility of this method applied to geochemistry and cosmochemistry for microanalysis.

Conflicts of interest

There are no conflicts to declare.

Acknowledgements

This study was financially supported by the Natural Science Foundation of China (Grant No. 41525012, 41973035 & 41903024), the National Key R&D Programmer of China (Grant No. 2016YFC0600109), the State Key Laboratory of Lithospheric Evolution (SKL-Z201901-YT), and the Scientific Instrument Developing Project of the Chinese Academy of Sciences (Grant No. YJKYYQ20170034). We are particularly thankful to Dr Yamirka Rojas-Agramonte for correcting the English. We are also grateful to two anonymous reviewers for critical and insightful comments that greatly improved this manuscript.

References

1 M. S. A. Horstwood, G. L. Foster, R. R. Parrish, S. R. Noble and G. M. Nowell, *J. Anal. At. Spectrom.*, 2003, **18**, 837–846.
2 R. N. Taylor, T. Warneke, J. A. Milton, I. W. Croudace, P. E. Warwick and R. W. Nesbitt, *J. Anal. At. Spectrom.*, 2003, **18**, 480–484.
3 K. Hattori, S. Sakata, M. Tanaka, Y. Orihashi and T. Hirata, *J. Anal. At. Spectrom.*, 2017, **32**, 88–95.
4 L. W. Xie, N. J. Evans, Y. H. Yang, C. Huang and J. H. Yang, *J. Anal. At. Spectrom.*, 2018, **33**, 1600–1615.
5 D. M. Chew, J. A. Petrus and B. S. Kamber, *Chem. Geol.*, 2014, **363**, 185–199.
6 A. J. Walder, I. Platzner and P. A. Freedman, *J. Anal. At. Spectrom.*, 1993, **8**, 19–23.
7 G. L. Foster and D. Vance, *J. Anal. At. Spectrom.*, 2006, **21**, 288–296.
8 F. Y. Wu, Y. H. Yang, L. W. Xie, J. H. Yang and P. Xu, *Chem. Geol.*, 2006, **234**, 105–126.

9 Y. H. Yang, F. Y. Wu, J. H. Yang, D. M. Chew, L. W. Xie, Z. Y. Chu, Y. B. Zhang and C. Huang, *Chem. Geol.*, 2014, **385**, 35–55.

10 C. M. Fisher, J. D. Vervoort and S. A. DuFrane, *Geochem., Geophys., Geosyst.*, 2014, **15**, 121–139.

11 T. M. Harrison, J. Blichert-Toft, W. Muller, F. Albarede, P. Holden and S. J. Mojzsis, *Science*, 2005, **310**, 1947–1950.

12 L. W. Xie, Y. B. Zhang, H. H. Zhang, J. F. Sun and F. Y. Wu, *Chin. Sci. Bull.*, 2008, **53**, 1565–1573.

13 H. L. Yuan, S. Gao, M. N. Dai, C. L. Zong, D. Gunther, G. H. Fontaine, X. M. Liu and C. Diwu, *Chem. Geol.*, 2008, **247**, 100–118.

14 D. L. Tollstrup, L. W. Xie, J. B. Wimpenny, E. Chin, C. T. Lee and Q. Z. Yin, *Geochem., Geophys., Geosyst.*, 2012, **13**, Q03017.

15 C. Huang, Y. H. Yang, J. H. Yang and L. W. Xie, *J. Anal. At. Spectrom.*, 2015, **30**, 994–1000.

16 C. J. Spencer, A. J. Cavosie, T. D. Raub, H. Rollinson, H. Jeon, M. P. Searle, J. A. Miller, B. J. McDonald, N. J. Evans and E. I. M. Facility, *Geology*, 2017, **45**, 975–978.

17 D. J. Goudie, C. M. Fisher, J. M. Hanchar, J. L. Crowley and J. C. Ayers, *Geochem., Geophys., Geosyst.*, 2014, **15**, 2575–2600.

18 B. R. Hacker, A. C. Kylander-Clark, R. Holder, T. B. Andersen, E. M. Peterman, E. O. Walsh and J. K. Munnikhuis, *Chem. Geol.*, 2015, **409**, 28–41.

19 M. A. Stearns, J. M. Cottle, B. R. Hacker and A. R. C. Kylander-Clark, *Chem. Geol.*, 2016, **422**, 13–24.

20 T. Prohaska, J. Irrgeher and A. Zitek, *J. Anal. At. Spectrom.*, 2016, **31**, 1612–1621.

21 C. M. Fisher, C. Paton, D. G. Pearson, C. Sarkar, Y. Luo, D. B. Tersmette and T. Chacko, *Geochem., Geophys., Geosyst.*, 2017, **18**, 4604–4622.

22 A. R. C. Kylander-Clark, B. R. Hacker and J. M. Cottle, *Chem. Geol.*, 2013, **345**, 99–112.

23 D. R. Viete, A. R. C. Kylander-Clark and B. R. Hacker, *Chem. Geol.*, 2015, **415**, 70–86.

24 J. Woodhead, J. Hergt, M. Shelley, S. Eggins and R. Kemp, *Chem. Geol.*, 2004, **209**, 121–135.

25 T. M. Harrison, A. K. Schmitt, M. T. McCulloch and O. M. Lovera, *Earth Planet. Sci. Lett.*, 2008, **268**, 476–486.

26 A. I. S. Kemp, G. L. Foster, A. Schersten, M. J. Whitehouse, J. Darling and C. Storey, *Chem. Geol.*, 2009, **261**, 244–260.

27 X. P. Xia, M. Sun, H. Y. Geng, Y. L. Sun, Y. J. Wang and G. C. Zhao, *J. Anal. At. Spectrom.*, 2011, **26**, 1868–1871.

28 G. Craig, A. J. Managh, C. Stremtan, N. S. Lloyd and M. S. A. Horstwood, *Goldschmidt Poster*, 2019.

29 Y. H. Yang, F. Y. Wu, Z. Y. Chu, L. W. Xie and J. H. Yang, *Spectrochim. Acta, Part B*, 2013, **79–80**, 82–87.

30 L. W. Xie, J. H. Yang, Q. Z. Yin, Y. H. Yang, J. B. Liu and C. Huang, *J. Anal. At. Spectrom.*, 2017, **32**, 975–986.

31 T. Iizuka and T. Hirata, *Chem. Geol.*, 2005, **220**, 121–137.

32 Z. C. Hu, Y. S. Liu, S. Gao, S. H. Hu, R. Dietiker and D. Gunther, *J. Anal. At. Spectrom.*, 2008, **23**, 1192–1203.

33 Y. H. Yang, J. F. Sun, L. W. Xie, H. R. Fan and F. Y. Wu, *Chin. Sci. Bull.*, 2008, **53**, 1062–1070.

34 Y. H. Yang, F. Y. Wu, S. A. Wilde, X. M. Liu, Y. B. Zhang, L. W. Xie and J. H. Yang, *Chem. Geol.*, 2009, **264**, 24–42.

35 Y. H. Yang, F. Y. Wu, L. W. Xie and Y. B. Zhang, *Anal. Lett.*, 2010, **43**, 142–150.

36 Y. H. Yang, Z. Y. Chu, F. Y. Wu, L. W. Xie and J. H. Yang, *J. Anal. At. Spectrom.*, 2011, **26**, 1237–1244.

37 Y. S. Liu, S. Gao, Z. C. Hu, C. G. Gao, K. Q. Zong and D. B. Wang, *J. Petrol.*, 2010, **51**, 537–571.

38 K. R. Ludwig, *User's Manual for Isoplot 3.00*, Berkeley Geochronol. Cent., Berkeley, Calif., 2003, p. 70.

39 Q. Ma, N. J. Evans, X. X. Ling, Y. J. Yang, F. W. Wu, Z. D. Zhao and Y. H. Yang, *Geostand. Geoanal. Res.*, 2019, **43**, 355–384.

40 J. N. Aleinikoff, W. S. Schenck, M. O. Plank, L. A. Srogi, C. M. Fanning, S. L. Kamo and H. Bosbyshell, *Geol. Soc. Am. Bull.*, 2006, **118**, 39–64.

41 E. M. Peterman, B. R. Hacker, M. Grove, G. E. Gehrels and J. M. Mattinson, *American Geophysical Union, Fall Meeting*, 2006, p. V21A-0551.

42 K. E. Alagna, M. Petrelli, D. Perugini and G. Poli, *Geostand. Geoanal. Res.*, 2008, **32**, 103–120.

43 Z. C. Liu, F. Y. Wu, Y. H. Yang, J. H. Yang and S. A. Wilde, *Chem. Geol.*, 2012, **334**, 221–239.

44 E. M. Peterman, J. M. Mattinson and B. R. Hacker, *Chem. Geol.*, 2012, **312**, 58–73.

45 G. O. Goncalves, C. Lana, R. Scholz, I. S. Buick, A. Gerdes, S. L. Kamo, F. Corfu, D. Rubatto, M. Wiedenbeck, H. A. Nalini and L. C. A. Oliveira, *Geostand. Geoanal. Res.*, 2018, **42**, 25–47.

46 X. X. Ling, M. H. Huyskens, Q. L. Li, Q. Z. Yin, R. Werner, Y. Liu, G. Q. Tang, Y. N. Yang and X. H. Li, *Mineral. Petrol.*, 2017, **111**, 163–172.

47 J. N. Aleinikoff, R. P. Wintsch, R. P. Tollo, D. M. Unruh, C. M. Fanning and M. D. Schmitz, *Am. J. Sci.*, 2007, **307**, 63–118.

48 A. K. Kenedy, S. L. Kamo, L. Nasdala and N. E. Timms, *Can. Mineral.*, 2010, **48**, 1423–1443.

49 J. F. Sun, J. H. Yang, F. Y. Wu, L. W. Xie, Y. H. Yang, Z. C. Liu and X. H. Li, *Chin. Sci. Bull.*, 2012, **57**, 2506–2516.

50 J. S. Stacey and J. D. Kramers, *Earth Planet. Sci. Lett.*, 1975, **26**, 207–221.

51 K. J. Spencer, B. R. Hacker, A. R. C. Kylander-Clark, T. B. Andersen, J. M. Cottle, M. A. Stearns, J. E. Poletti and G. G. E. Seward, *Chem. Geol.*, 2013, **341**, 84–101.

52 F. Y. Wu, A. A. Arzamastsev, R. H. Mitchell, Q. L. Li, J. Sun, Y. H. Yang and R. C. Wang, *Chem. Geol.*, 2013, **353**, 210–229.

53 F. Y. Wu, Y. H. Yang, M. A. W. Marks, Z. C. Liu, Q. Zhou, W. C. Ge, J. S. Yang, Z. F. Zhao, R. H. Mitchell and G. Markl, *Chem. Geol.*, 2010, **273**, 8–34.

54 F. Y. Wu, Y. H. Yang, R. H. Mitchell, F. Bellatreccia, Q. L. Li and Z. F. Zhao, *Chem. Geol.*, 2010, **277**, 178–195.

55 F. Y. Wu, Y. H. Yang, R. H. Mitchell, Q. L. Li, J. H. Yang and Y. B. Zhang, *Lithos*, 2010, **115**, 205–222.

56 Y. H. Yang, F. Y. Wu, Y. Li, J. H. Yang, L. W. Xie, Y. Liu, Y. B. Zhang and C. Huang, *J. Anal. At. Spectrom.*, 2014, **29**, 1017–1023.

57 Y. H. Yang, F. Y. Wu, J. H. Yang, R. H. Mitchell, Z. F. Zhao, L. W. Xie, C. Huang, Q. Ma, M. Yang and H. Zhao, *J. Anal. At. Spectrom.*, 2018, **33**, 231–239.

58 Y. H. Yang, F. Y. Wu, Q. L. Li, Y. Rojas-Agramonte, J. H. Yang, Y. Li, Q. Ma, L. W. Xie, C. Huang, H. R. Fan, Z. F. Zhao and C. Xu, *Geostand. Geoanal. Res.*, 2019, **43**, 543–565.